

The NLO QCD corrections to $B_c(B_c^*)$ production around Z pole at an e^+e^- collider

Xu-Chang Zheng^{a,c*}, Chao-Hsi Chang^{a,b,c†}, Tai-Fu Feng^{a,d‡}, Zan Pan^{a,c§}

^a Key Laboratory of Theoretical Physics, Institute of Theoretical Physics,
Chinese Academy of Sciences, Beijing 100190, China

^b CCAST (World Laboratory), P.O.Box 8730, Beijing 100190 China

^c School of Physical Sciences, University of Chinese Academy of Sciences, Beijing 100049, China and

^d Department of Physics, Hebei University, Baoding, 071002, China

The production of B_c and B_c^* mesons at Z -factory (an e^+e^- collider running at energies around Z pole) is calculated up-to the next-to-leading order (NLO) QCD corrections. The results show that the dependence of the total cross sections on the renormalization scale μ is suppressed by the corrections, and the NLO corrections enhance the total cross sections for B_c by 52% and for B_c^* by 33%, when the renormalization scale is taken at $\mu = 2m_b$. To observe B_c and B_c^* mesons, the differential cross section on the out-going angle and the distribution on the energy fraction z both up-to QCD NLO accuracy as well as the relevant K -factor (NLO to LO) for the production are computed and obtained results are presented properly.

Keywords: B_c meson, production, Z -factory

PACS numbers: 13.66.Bc, 13.87.Fh, 14.70.Hp, 14.40.-n, 14.20.-c,

I. INTRODUCTION

The meson B_c (and its anti-particle \bar{B}_c), being an explicitly heavy-flavored quark-antiquark ground state, is unique in the Standard Model (SM), and attracts a lot of interests, particularly after its first observation by CDF collaboration[1]. The two components inside it move non-relativistically due to its doubly heavy flavor nature, so potential model can describe it reliably[2], while the nonrelativistic quantum chromodynamics effective theory (NRQCD) may be used to compute its production[3], and the effective theory for the weak interaction which is based on SM may be used to compute its decays.

Since the available observations on it are only those at high energy hadronic colliders so far, so the theoretical and experimental studies of the B_c production mainly focus on its hadronic production[4, 5]. However, the hadronic production of a hadron, e.g. B_c meson, always is through a collision of the partons inside the colliding hadrons, i.e. via a subprocess, the longitudinal components of the momenta of the products and the center-of-mass system of collision cannot be controlled ('not measurable'), so only the measurable perpendicular components of the momenta of the products may be properly to use in studying the subprocess. Moreover, at hadronic colliders, there are many hadrons in the final state of the concerned process which directly relate to the initial hadrons, but not relevant to the subprocess for the production, so they cause backgrounds only. On the contrary, at an e^+e^- collider there are less backgrounds

for the production, and the center-of-mass system of the collision is that of $e^+ + e^-$, i.e. well known, so all the momentum components of products, as well as the angle distributions of the concerned product(s) to the colliding e^+ or e^- are properly relevant to the production and they can be used to test theoretical predictions, thus to study B_c meson production at an e^+e^- collider is very interesting. Especially now several proposals about Z -factories (e^+e^- colliders running at energies around Z pole) with much higher luminosity than that of LEP-I, e.g. ILC, CEPC and FCC-ee, are under consideration, thus it is the time to re-study the production of B_c by e^+e^- collision, although from theoretical estimate[6] and experimental observations[7], it is found that the B_c meson production at LEP-I is too small to be observed.

Hence recently the production of doubly heavy flavored hadrons (B_c meson and baryons $\Xi_{cc}, \Xi_{bc}, \Xi_{bb}$ etc and their excited states as well as their antiparticle) via e^+e^- collision at the energy of Z pole mainly via Z -boson resonance is re-studied under the approach of complete QCD at the leading order (LO) and the fragmentation approach at the leading logarithm order (LL) thoroughly, and it is found that the LO results have quite remarkable dependence on the renormalization scale[8]. In order to have more precise theoretical prediction and to suppress the dependence on the renormalization scale, it is certainly interesting to carry out the computations on the B_c meson production at an e^+e^- collider up-to the QCD NLO accuracy.

Since B_c and its excited states B_c^*, \dots carry two heavy-flavors explicitly, so the excited states B_c^*, \dots will decay (or cascade-decay) to the ground state, B_c , through strong or electromagnetic interaction with almost 100% probability, thus as Ref.[8], here the production of the excited state B_c^* ($^3S_1, J^P = 1^-$, the lowest excited state of B_c , is also computed up-to QCD NLO.

We should note here that the production of $B_c(B_c^*)$ me-

*e-mail:zhengxc@itp.ac.cn

†e-mail:zhangzx@itp.ac.cn

‡email:fengt@hbu.edu.cn

§e-mail:panzan@itp.ac.cn

son at a Z -factory, $e^+e^- \rightarrow B_c(B_c^*) + \bar{c} + b$ at Z pole resonance, contains more information in physics to compare with that directly via Z decay, $Z \rightarrow B_c(B_c^*) + \bar{c} + b$. For instance, one may do the tests of the production at a Z -factory not only on the total cross-sections but also on the various differential cross-sections (the angle distributions, the forward-backward and lefthanded-righthanded asymmetries of the products to the direction of the initial electron or positron etc), therefore, in Ref.[8] the total cross-section and several differential cross-sections as well for the production are precisely presented. As the same reason and natural further development, here we do the calculations for the production via e^+e^- collision (at a Z -factory) up-to the next leading order (NLO) QCD accuracy, although the production directly via Z -decay up-to the NLO QCD corrections is available in Refs.[9, 10]. Indeed besides there is more information in physics, and the calculations on the production of the e^+e^- collision are much more complicated than those on the production directly via Z decay (especially that up-to NLO QCD accuracy). In fact, one can extract the relevant decay width from the total cross section of the production via e^+e^- collision precisely. Thus we do the extraction so as to compare the widths extracted from the calculations on the total cross sections obtained here with those available in Refs.[9, 10] carefully.

According to NRQCD[3], the production of $B_c(B_c^*)$ meson by electron-positron collisions can be factorized into two factors at a specific energy μ_F in QCD perturbative region: one is the electron-positron production of 'free' c, \bar{b} quark pair inclusively in short distance, which can be calculated by perturbative QCD (pQCD), and the other one is that to depict how to form the meson $B_c(B_c^*)$ from the produced c, \bar{b} quark pair. The later factor is nonperturbative, but can be achieved phenomenologically or via potential model (the wave function at origin) etc. Here we compute the production up-to next leading order (NLO) QCD corrections on the former factor, the leading order in relative velocity v between the two heavy quarks inside the meson $B_c(B_c^*)$ on the later factor and the factorization energy scale μ_F is set to be equal to the renormalization one μ_R . For convenience, later on we denote $\mu \equiv \mu_F = \mu_R$ throughout the paper.

The results in Ref.[8] for the production of doubly heavy flavored hadrons (B_c meson and baryons $\Xi_{cc}, \Xi_{bc}, \Xi_{bb}$ etc and their excited states as well as their antiparticle) at a Z -factory are obtained under complete QCD approach to leading order (LO) and fragmentation approach to leading logarithm order (LL), and the conclusion is achieved that if one wishes to study B_c or B_c^* (and higher excited states) meson thoroughly the luminosity for the e^+e^- collider running at the Z pole should be so high as $10^{35}\text{cm}^{-2}\text{s}^{-1}$ (even higher). While the present results for the production up-to the NLO QCD accuracy do not affect the conclusion much, owing to the NLO corrections do not change the results for the considered production too much.

The paper is organised as follows: Following the In-

roduction, in Section II, we present the formulas to the LO accuracy briefly. In Section III, we present the approaches to compute the NLO corrections of QCD for the B_c (and B_c^*) meson production at e^+e^- colliders. In Section IV, with the necessary parameters given the numerical results are presented. Section V is devoted to discussions and summary. In Appendix-A, it is shown how the relevant widths of the production of B_c meson and B_c^* meson by Z decay are derived from the total cross sections of the production by $e^+ + e^-$ collision and in Appendix-B precise comparisons between the derived widths via the total cross sections for $e^+ + e^-$ collision on the present computations and those by computing the production by Z decay directly in literature.

II. THE CROSS SECTION UP-TO LEADING ORDER (LO)

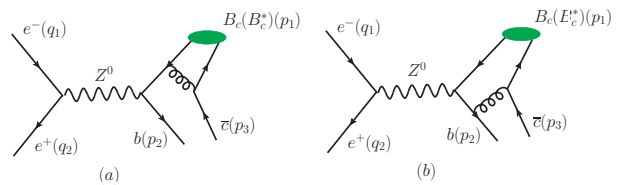


FIG. 1: Two of the four Feynman diagrams to LO accuracy for the production $e^-(q_1) + e^+(q_2) \rightarrow B_c(B_c^*)(p_1) + b(p_2) + \bar{c}(p_3)$.

There are four Feynman diagrams for the B_c and B_c^* production at LO accuracy, only two of them are presented in Fig.1, but the other two can be obtained by interchanging the b -quark and c -quark lines in Fig.1.

Note that in the present paper the studies focus on the production from QCD LO accuracy up-to QCD NLO accuracy, but merely when the $e^+ + e^-$ collider runs around the Z pole. Thus the contributions corresponding to the Feynman diagrams with Z -boson exchange are dominant and we will compute them carefully, but those corresponding to the Feynman diagrams with γ exchange are approximately ignored¹. Under the approximation the computations for QCD LO and QCD NLO are simplified quite a lot, and at the end of Section IV we also estimate how well the approximation is by taking into account the contributions from the Feynman diagrams with γ exchange, i.e. those from the γ exchange itself being squared and those due to the interference of the γ exchange and Z -boson exchange.

The cross section up-to LO QCD can be formulated as:

$$d\sigma_{\text{LO}} = \frac{1}{4} \frac{1}{s} \sum |M_{\text{LO}}|^2 d\Phi_3, \quad (1)$$

¹ Thus without special statement, in the Feynman diagrams Figs.1,2,3,4,5,6 the Z exchange diagrams are involved only, but the ones with the γ exchange are not.

where $\frac{1}{2s}$ is the flux factor. \sum means that the spins and the colors in the initial and final states are summed over. $1/4$ comes from the spin average of the initial e^+e^- . $d\Phi_3$ denotes the three-body phase space for the final states. M_{LO} is the LO Feynman amplitude, which is the sum of four terms for the LO Feynman diagrams. The details about M_{LO} can be found in Ref.[8].

III. THE NLO QCD CORRECTIONS

The NLO QCD corrections for the process $e^+ + e^- \rightarrow B_c(B_c^*) + b + \bar{c}$ include virtual and real ones. The half of the Feynman diagrams for the virtual correction are those

in Figs.2,3,4,5, and the half of the Feynman diagrams for the real correction are those in Fig.6. The other half of the Feynman diagrams also for the virtual corrections and for real corrections can be obtained by interchanging the b -quark and c -quark lines in Figs.2~6.

To the QCD NLO accuracy, the cross section is formulated as

$$\sigma_{\text{NLO}} = \sigma_{\text{LO}} + \sigma_{\text{Virtual}} + \sigma_{\text{Real}}. \quad (2)$$

Here σ_{Virtual} denotes the so-called virtual correction and σ_{Real} denotes the so-called real correction. Now let us calculate them respectively.

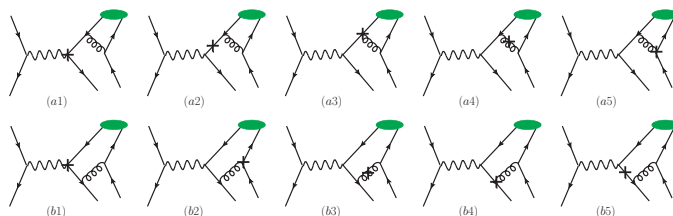


FIG. 2: Half of the counterterm diagrams for the process $e^- + e^+ \rightarrow B_c(B_c^*) + b + \bar{c}$.

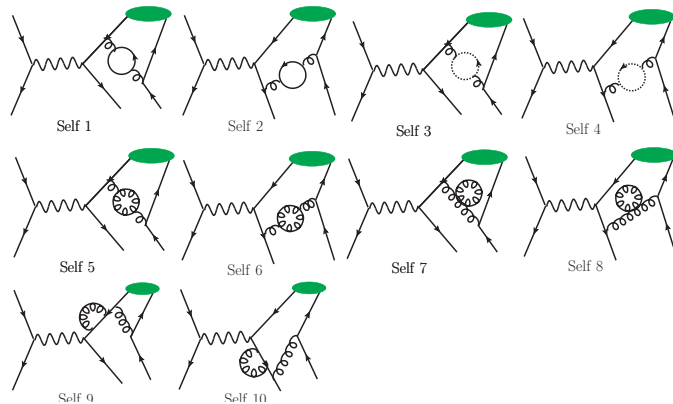


FIG. 3: Half of self-energy diagrams in the virtual correction.

A. The NLO QCD virtual correction

The virtual correction up-to QCD NLO is to consider the interference of the LO ones and those corresponding to the correction Feynman diagrams, i.e. Figs.2,3,4,5 and those with the c -quark and b -quark lines being interchanged. Thus the virtual correction to the cross section can be formulated as

$$d\sigma_{\text{Virtual}} = \frac{1}{4} \frac{1}{2s} \sum 2\text{Re}(M_{\text{LO}}^* M_{\text{Virtual}}) d\Phi_3. \quad (3)$$

There are ultraviolet (UV) and infrared (IR) diver-

gences in the amplitudes corresponding to the correction Feynman diagrams. We adopt dimensional regularization with $D = 4 - 2\epsilon$ to isolate the UV and IR divergences. There are the Coulomb divergences in the conventional matching procedure, which should be absorbed into the binding potential for the two heavy quarks inside the B_c and B_c^* . In the dimensional regularization, there is a simpler way to extract the NRQCD short-distance coefficients directly using the method of regions[11], i.e., expanding the amplitudes with the relative momentum (q) of the constituent quarks before performing loop inte-

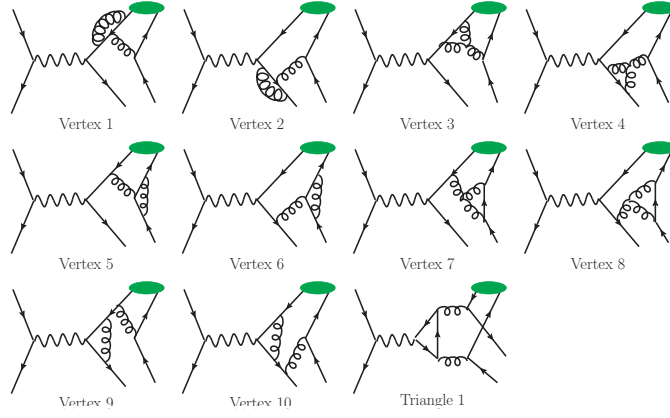


FIG. 4: Half of vertex and triangle diagrams in the virtual correction.

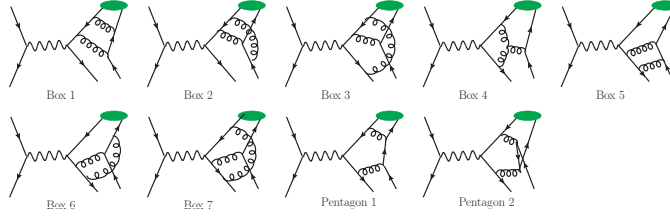


FIG. 5: Half of box and pentagon diagrams in the virtual correction.

gration, and in the lowest non-relativistic approximation for the S -wave states of the binding system $c\bar{b}$, only the terms with $q = 0$ are taken. Thus we don't confront the contributions from the low energy regions such as those from the potential region.

In dimensional regularization, γ_5 should be treated carefully. We adopt the reading point prescription[12]. It has the following rules,

- The anticommutation relation $\{\gamma_5, \gamma^\mu\} = 0$ is valid. Thus after applying the anticommutation relation and $\gamma_5^2 = 1$, there is one or no γ_5 in each Dirac trace.
- Cyclic manipulation in the Dirac traces is prevented. When considering the contributions from several diagrams, for all of them the traces in the amplitude (or resulting from squared fermionic amplitudes) must be read with starting from the same vertex respectively.
- The relevant axial current anomalies would be obtained and the conservation for vector currents is guaranteed by starting all the traces with the axial vector vertex.

Here the UV divergences come from self-energy, vertex and triangle diagrams only², which are canceled by

the counterterms through renormalization, and here the renormalization scheme is that the renormalization constants Z_2 , Z_m , and Z_3 , which correspond to the renormalization of quark field, quark mass and gluon field, are determined by the renormalization of the on-mass-shell scheme (OS), whereas Z_g relating to the strong coupling constant α_s is determined by the renormalization of the modified-minimal-subtraction scheme (\overline{MS}). Then with the renormalization, we have:

$$\begin{aligned}
 \delta Z_2^{OS} &= -C_F \frac{\alpha_s}{4\pi} \left[\frac{1}{\epsilon_{UV}} + \frac{2}{\epsilon_{IR}} - 3\gamma_E + 3 \ln \frac{4\pi\mu^2}{m^2} + 4 \right], \\
 \delta Z_m^{OS} &= -3 C_F \frac{\alpha_s}{4\pi} \left[\frac{1}{\epsilon_{UV}} - \gamma_E + \ln \frac{4\pi\mu^2}{m^2} + \frac{4}{3} \right], \\
 \delta Z_3^{OS} &= \frac{\alpha_s}{4\pi} \left[(\beta'_0 - 2C_A) \left(\frac{1}{\epsilon_{UV}} - \frac{1}{\epsilon_{IR}} \right) \right. \\
 &\quad \left. - \frac{4}{3} T_F \left(\frac{1}{\epsilon_{UV}} - \gamma_E + \ln \frac{4\pi\mu^2}{m_c^2} \right) \right. \\
 &\quad \left. - \frac{4}{3} T_F \left(\frac{1}{\epsilon_{UV}} - \gamma_E + \ln \frac{4\pi\mu^2}{m_b^2} \right) \right], \\
 \delta Z_g^{\overline{MS}} &= -\frac{\beta_0}{2} \frac{\alpha_s}{4\pi} \left[\frac{1}{\epsilon_{UV}} - \gamma_E + \ln(4\pi) \right], \tag{4}
 \end{aligned}$$

where m appearing in δZ_2^{OS} and δZ_m^{OS} represents the mass m_b or m_c accordingly, μ is the energy where the

² The UV divergence from the amplitude of the anomalous dia-

gram Triangle-1 in Fig.4 is canceled by the UV divergence from the other anomalous diagram.

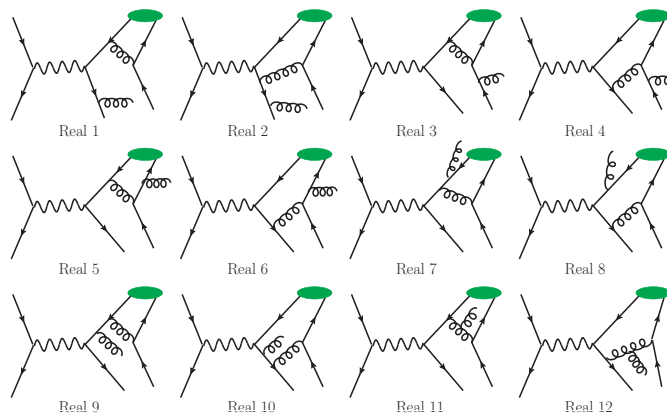


FIG. 6: Half of the Feynman diagrams in the real correction.

renormalization is carried out, and γ_E is Euler's constant. $\beta_0 = \frac{11}{3}C_A - \frac{4}{3}T_F n_f$ is the one-loop coefficient of the QCD β -function, and n_f is the number of active quark flavors. Here for the concerned process, there are three light quarks u, d, s and two heavy quarks c, b , so $n_f = 5$. But in Eq.(4) precisely $\beta'_0 = \frac{11}{3}C_A - \frac{4}{3}T_F n_{lf}$, and $n_{lf} = 3$ for the light quark flavors. For $SU(3)_c$ group, $C_A = 3$, $T_F = \frac{1}{2}$ and $C_F = \frac{4}{3}$. Because there is no external gluon line at LO level, δZ_3 is canceled at NLO total amplitude level, so the final results are independent of the renormalization scheme of the gluon field.

The IR divergences in the Feynman diagrams for the virtual correction can be well analyzed[13, 14]. For the concerned process, the IR divergences come from the vertex, box and pentagon diagrams. Of Fig.4, only the amplitudes corresponding to diagrams Vertex-5 and Vertex-6 have IR divergences. Of Fig.5, except Box-4, the rests have IR divergences³. The other half of the Feynman diagrams, which are obtained from Figs.4~5 by interchanging the c -quark and b -quark lines, have similar IR divergences. The IR divergences in the virtual correction will be canceled by the IR divergences from the counterterms and the real correction.

B. The real corrections to NLO

Note that here 'the NLO real correction'⁴ for the concerned process $e^- + e^+ \rightarrow B_c(B_c^*) + b + \bar{c}$ means to take into account the full contributions from the process $e^-(q_1) + e^+(q_2) \rightarrow B_c(B_c^*)(p_1) + b(p_2) + \bar{c}(p_3) + g(p_4)$ with an additional gluon in final state but covering whole possible phase space.

³ We find that combinations Vertex-5 + Box-2, Vertex-6 + Box-3 + Pentagon-2 and Box-6 + Box-7 are IR finite. This is similar to the B_c production through Z-decay in Refs.[9, 10].

⁴ In literature, sometimes 'the NLO real correction' contains only the contributions from the process $e^+e^- \rightarrow B_c(B_c^*) + b + \bar{c} + g$ with the gluon g so soft or collinear to merge into b or \bar{c} jet.

Half of the Feynman diagrams for the real correction are shown in Fig.6 and the other half can be obtained from Fig.6 through interchanging the c -quark and b -quark lines. The correction to the relevant cross section can be written as:

$$d\sigma_{\text{Real}} = \frac{1}{4} \frac{1}{2s} \sum |M_{\text{Real}}|^2 d\Phi_4, \quad (5)$$

where M_{Real} is the sum of 24 terms relating to the 24 Feynman diagrams for the real correction. $|M_{\text{Real}}|^2$ can be formulated as

$$|M_{\text{Real}}|^2 = \sum_{i,j} M_{\text{Real},i}^* M_{\text{Real},j}, \quad (6)$$

where i, j vary from 1 to 24 corresponding to the 24 real correction Feynman diagrams.

There are IR divergences in the real correction, which are generated by the phase space integration, and they should be finally canceled by the IR divergences appearing in the virtual correction. It is easy to realize[?] that, the terms $M_{\text{Real},i}^* M_{\text{Real},j}$ are IR finite for the phase space integration unless $M_{\text{Real},i}$ and $M_{\text{Real},j}$ are the amplitudes corresponding to Feynman diagrams in which a real gluon is emitted from an external on-shell line, e.g., here the first 8 diagrams in Fig.6. At this step, let us divide the cross section of the real correction into two parts as

$$d\sigma_{\text{Real}} = d\sigma_{\text{Real}}^{\text{IR}} + d\sigma_{\text{Real}}^{\text{IR-finite}}, \quad (7)$$

where $d\sigma_{\text{Real}}^{\text{IR}}$ contains the terms in $\sum_{i,j} M_{\text{Real},i}^* M_{\text{Real},j}$ only when $M_{\text{Real},i}$ and $M_{\text{Real},j}$ are the amplitudes corresponding to Feynman diagrams in which a real gluon is emitted from an external on-shell line. Namely we can formulate $d\sigma_{\text{Real}}^{\text{IR}}$ as

$$d\sigma_{\text{Real}}^{\text{IR}} = \frac{1}{4} \frac{1}{2s} \sum |M_{\text{Real}}^{\text{IR}}|^2 d\Phi_4 \quad (8)$$

where $M_{\text{Real}}^{\text{IR}}$ is the sum of the amplitudes corresponding to Feynman diagrams in which a real gluon is emitted

from an external on-shell line. $d\sigma_{\text{Real}}^{\text{IR-finite}}$ contains the remaining terms in $\sum_{i,j} M_{\text{Real},i}^* M_{\text{Real},j}$, i.e., $(|M_{\text{Real}}|^2 - |M_{\text{Real}}^{\text{IR}}|^2)$. Due to the fact that there is no divergence in $\sigma_{\text{Real}}^{\text{IR-finite}}$, we can calculate it in 4-dimensional space-time directly.

In order to extract the IR divergences in $\sigma_{\text{Real}}^{\text{IR}}$ precisely so as to cancel the IR divergences in virtual correction precisely, we adopt the two-cutoff phase space slicing method[16]. By this method, the integration on the phase space is divided into two sectors through introducing a very soft cut $\delta_s (\ll 1)$ on the energy of the emitting gluon (p_4^0). Then,

$$d\sigma_{\text{Real}}^{\text{IR}} = d\sigma_{\text{Real}}^{\text{IR,soft}} + d\sigma_{\text{Real}}^{\text{IR,hard}}, \quad (9)$$

where

$$d\sigma_{\text{Real}}^{\text{IR,hard}} = \frac{1}{4} \frac{1}{2s} \sum |M_{\text{Real}}^{\text{IR}}|^2 d\Phi_4|_{p_4^0 > \delta_s \sqrt{s}/2}, \quad (10)$$

and

$$d\sigma_{\text{Real}}^{\text{IR,soft}} = \frac{1}{4} \frac{1}{2s} \sum |M_{\text{Real}}^{\text{IR}}|^2 d\Phi_4|_{p_4^0 < \delta_s \sqrt{s}/2}. \quad (11)$$

To calculate $\sigma_{\text{Real}}^{\text{IR,soft}}$, the eikonal approximation is adopted to deal with the amplitudes involved in $M_{\text{Real}}^{\text{IR}}$, where the terms of $\mathcal{O}(\delta_s)$ in $\sigma_{\text{Real}}^{\text{IR,soft}}$ have been neglected [16, 17]. Under this approximation, the amplitude corresponding to the Feynman diagram where a real gluon emitted from an external line can be factorized as a Born factor multiplying an eikonal factor, and it is easy to check that the eikonal factors relating to the diagrams Real-5 and Real-6 of Fig.6 are canceled by the eikonal factors relating to the diagrams Real-7 and Real-8 of Fig.6 respectively at the leading order approximation in relative velocity $\mathcal{O}(v^0)$. Thus at last under the eikonal approximation we obtain

$$\sum |M_{\text{Real}}^{\text{IR}}|^2 = 4\pi\alpha_s C_F \mu^{2\epsilon} \left[\frac{-(p_2)^2}{(p_2 \cdot p_4)^2} + \frac{2p_2 \cdot p_3}{(p_2 \cdot p_4)(p_3 \cdot p_4)} - \frac{(p_3)^2}{(p_3 \cdot p_4)^2} \right] \sum |M_{\text{Born}}|^2. \quad (12)$$

Up-to corrections of $\mathcal{O}(\delta_s)$, the phase space for the soft sector can be factorized as [16]

$$d\Phi_4|_{p_4^0 < \delta_s \sqrt{s}/2} = d\Phi_3 \frac{d^{d-1} p_4}{2p_4^0 (2\pi)^{d-1}} |_{p_4^0 < \delta_s \sqrt{s}/2} \quad (13)$$

where $d\Phi_3$ denotes the element of the three-body phase space without emitting a gluon. Performing the integration over the momentum of the emitting gluon (p_4) in the soft sector, the differential cross section

$$d\sigma_{\text{Real}}^{\text{IR,soft}} = d\sigma_{\text{Born}} \frac{\alpha_s}{\pi} \Gamma(1 + \epsilon) \left(\frac{4\pi\mu^2}{s} \right)^\epsilon \left(\frac{A}{\epsilon} + B \right) \quad (14)$$

is obtain[18], where

$$\begin{aligned} A &= C_F \left[1 - \frac{\kappa (p_2 \cdot p_3)}{\kappa^2 m_b^2 - m_c^2} \ln \left(\frac{\kappa^2 m_b^2}{m_c^2} \right) \right], \\ B &= C_F \left\{ - \left[1 - \frac{\kappa (p_2 \cdot p_3)}{\kappa^2 m_b^2 - m_c^2} \ln \left(\frac{\kappa^2 m_b^2}{m_c^2} \right) \right] \ln(\delta_s^2) + \frac{1}{2\beta_b} \ln \left(\frac{1 + \beta_b}{1 - \beta_b} \right) + \frac{1}{2\beta_{\bar{c}}} \ln \left(\frac{1 + \beta_{\bar{c}}}{1 - \beta_{\bar{c}}} \right) \right. \\ &\quad \left. + \frac{2\kappa (p_2 \cdot p_3)}{\kappa^2 m_b^2 - m_c^2} \left[\frac{1}{4} \ln^2 \left(\frac{u^0 - |\mathbf{u}|}{u^0 + |\mathbf{u}|} \right) + \text{Li}_2 \left(1 - \frac{u^0 + |\mathbf{u}|}{v} \right) + \text{Li}_2 \left(1 - \frac{u^0 - |\mathbf{u}|}{v} \right) \right]_{u=p_3}^{u=\kappa p_2} \right\}, \quad (15) \end{aligned}$$

here

$$\begin{aligned} \beta_b &= \sqrt{1 - m_b^2/(p_2^0)^2}, \\ \beta_{\bar{c}} &= \sqrt{1 - m_c^2/(p_3^0)^2}, \end{aligned} \quad (16)$$

$$v = \frac{\kappa^2 m_b^2 - m_c^2}{2(\kappa p_2^0 - p_3^0)}, \quad (17)$$

and

$$\kappa = \frac{p_2 \cdot p_3 + \sqrt{(p_2 \cdot p_3)^2 - m_b^2 m_c^2}}{m_b^2}. \quad (18)$$

It can be checked precisely that the $1/\epsilon$ -terms in $d\sigma_{\text{Real}}^{\text{IR,soft}}$ defined by Eq.(14) are just canceled by those infrared $1/\epsilon$ -terms remained by the virtual correction Eq.(3).

Since there is no IR divergence in $d\sigma_{\text{Real}}^{\text{IR,hard}}$ due to the constraint $p_4^0 > \delta_s \sqrt{s}/2$, so we can calculate it in 4-

$\cos\theta$	-0.8	-0.6	-0.4	-0.2	0	0.2	0.4	0.6	0.8
$d\sigma/d\cos\theta(B_c, LO)$	1.066	0.892	0.759	0.667	0.617	0.608	0.639	0.711	0.825
$d\sigma/d\cos\theta(B_c, NLO)$	1.606	1.346	1.150	1.014	0.939	0.924	0.969	1.075	1.242
$K(B_c)$	1.506	1.509	1.515	1.520	1.522	1.520	1.516	1.512	1.505
$d\sigma/d\cos\theta(B_c^*, LO)$	1.507	1.254	1.060	0.926	0.853	0.839	0.884	0.990	1.156
$d\sigma/d\cos\theta(B_c^*, NLO)$	1.990	1.662	1.414	1.240	1.144	1.125	1.183	1.317	1.529
$K(B_c^*)$	1.320	1.325	1.334	1.339	1.341	1.341	1.338	1.330	1.323

TABLE III: The LO and NLO differential cross sections $\frac{d\sigma}{d\cos\theta}$ (in pb) of $e^-e^+ \rightarrow B_c(B_c^*) + b + \bar{c} + X$ and their ratio at various scattering angles ($\cos\theta$) at the Z pole ($\mu = 2m_b$).

dimensional space-time safely. Summing up $\sigma_{\text{Real}}^{\text{IR-soft}}$, $\sigma_{\text{Real}}^{\text{IR,hard}}$ and $\sigma_{\text{Real}}^{\text{IR-finite}}$, the requested σ_{Real} is obtained. Then with the Eqs.(2,3,7), the cross section σ_{NLO} of the process $e^+e^- \rightarrow B_c(B_c^*) + b + \bar{c} + X$, i.e. the production to QCD NLO accuracy, is achieved.

IV. NUMERICAL RESULTS

For numerical calculations, the necessary input parameters are taken as follows:

$$\begin{aligned}
m_b &= 4.9 \text{ GeV}, \quad m_c = 1.5 \text{ GeV}, \quad m_Z = 91.1876 \text{ GeV}, \\
\sin^2\theta_w &= 0.231, \quad \alpha = 1/128, \quad \Gamma_Z = 2.4952 \text{ GeV}, \\
|R_S(0)|^2 &= 1.642 \text{ GeV}^3,
\end{aligned} \tag{19}$$

$\alpha = \alpha(m_Z)$ is the electromagnetic coupling constant at $\mu = m_Z$; $R_S(0)$ is the radial wave function at the origin for $B_c(B_c^*)$, which can be taken from the potential model[2]. We apply the two-loop formula for the strong coupling constant $\alpha_s(\mu)$:

$$\alpha_s(\mu) = \frac{4\pi}{\beta_0 \ln(\mu^2/\Lambda_{QCD}^2)} \left[1 - \frac{\beta_1 \ln \ln(\mu^2/\Lambda_{QCD}^2)}{\beta_0^2 \ln(\mu^2/\Lambda_{QCD}^2)} \right], \tag{20}$$

Note that in the calculations here, we use FeynArts[20] for generating Feynman diagrams and amplitudes, FeynCalc[21] and FeynCalcFormLink[22] for carrying out the trace of color and Dirac matrices; while Apart[23] and FIRE[24] for conducting partial fraction and integration-by-parts (IBP) reduction. All the one-loop integrals are reduced into master integrals and the master integrals are computed in terms of LoopTools[25] numerically. The final phase-space integrations are computed with the help of the soft-ware Vegas[26].

The numerical results of the total cross sections at the colliding center-mass energy m_Z as well as the so-called K -factor (QCD) for the productions $e^+e^- \rightarrow B_c + b + \bar{c} + X$ and $e^+e^- \rightarrow B_c^* + b + \bar{c} + X$ with two different renormalization scales, $\mu = 2m_b$ and $\mu = m_Z/2$, are put

where $\beta_1 = \frac{34}{3}C_A^2 - 4C_F T_F n_f - \frac{20}{3}C_A T_F n_f$ is the two-loop coefficient of the QCD β -function. According to $\alpha_s(m_Z) = 0.1185$ [19], we obtain $\Lambda_{QCD}^{n_f=5} = 0.233 \text{ GeV}$.

μ	$\alpha_s(\mu)$	$\sigma_{\text{LO}}(\text{pb})$	$\sigma_{\text{NLO}}(\text{pb})$	$K \equiv \sigma_{\text{NLO}}/\sigma_{\text{LO}}$
$2m_b$	0.180	1.576	2.387	1.515
$m_Z/2$	0.132	0.847	1.587	1.874

TABLE I: The total cross section of $e^+e^- \rightarrow B_c + b + \bar{c} + X$ at Z pole with two typical renormalization scales.

μ	$\alpha_s(\mu)$	$\sigma_{\text{LO}}(\text{pb})$	$\sigma_{\text{NLO}}(\text{pb})$	$K \equiv \sigma_{\text{NLO}}/\sigma_{\text{LO}}$
$2m_b$	0.180	2.204	2.930	1.329
$m_Z/2$	0.132	1.185	2.059	1.738

TABLE II: The total cross section of $e^+e^- \rightarrow B_c^* + b + \bar{c} + X$ at Z pole with two typical renormalization scales.

into the tables: TABLE I and TABLE II respectively, and the precise dependence of the cross sections on the renormalization scale μ for LO and NLO QCD is presented in Fig.7. It is shown in Fig.7 that the cross section of the production $e^+e^- \rightarrow B_c(B_c^*) + b + \bar{c} + X$ at Z pole decreases by 46%(46%) at LO but by 34% (30%) at NLO when the renormalization scale μ changes from $2m_b$ to $m_Z/2$. Namely the dependence on renormalization scale μ is weakened a lot due to NLO correction. Whereas the dependence on the renormalization scale μ is still quite great for NLO, thus it seems that, to suppress the dependence on μ further, higher order corrections in QCD for the concerned production are requested.

Moreover, we also with $\mu = 2m_b$ calculate the differential cross sections $d\sigma/d\cos\theta$, $d\sigma/dz$ and the relevant K -

z	0.183	0.269	0.355	0.441	0.527	0.613	0.699	0.785	0.871	0.957
$d\sigma/dz(B_c, LO)$	0.276	0.543	0.833	1.195	1.655	2.237	2.932	3.603	3.664	1.534
$d\sigma/dz(B_c, NLO)$	0.650	1.173	1.682	2.274	2.964	3.732	4.508	4.970	4.360	1.578
$K(B_c)$	2.355	2.160	2.019	1.903	1.791	1.668	1.538	1.379	1.190	1.029
$d\sigma/dz(B_c^*, LO)$	0.167	0.417	0.699	1.091	1.681	2.582	3.905	5.584	6.617	3.187
$d\sigma/dz(B_c^*, NLO)$	0.446	0.920	1.418	2.029	2.884	4.098	5.586	7.056	7.058	2.852
$K(B_c^*)$	2.671	2.206	2.029	1.860	1.716	1.587	1.430	1.264	1.067	0.895

TABLE IV: The LO and NLO differential cross sections $\frac{d\sigma}{dz}$ (in pb) of $e^-e^+ \rightarrow B_c(B_c^*) + b + \bar{c} + X$ and their ratio at various values of z at the Z pole ($\mu = 2m_b$).

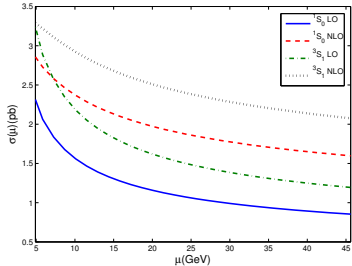


FIG. 7: The dependence of the total cross sections for $B_c(B_c^*)$ production on the renormalization scale μ at the Z pole to LO and NLO.

factor as well. Here θ is the angle between the momenta of the electron in initial state and the meson $B_c(B_c^*)$ in final state at center-of-mass system of the e^+, e^- collision and z is the ‘energy-fraction’ defined as $2k \cdot p_1/s$ (k is the momentum carried by Z boson).

The differential cross sections $d\sigma/d\cos\theta$ for the production of $B_c(B_c^*)$ meson with $\mu = 2m_b$ to LO and NLO, and the K factor as well are put in TABLE III. The differential cross section $d\sigma/d\cos\theta$ with renormalization scale $\mu = 2m_b$ is presented in Fig.8. One can see from Fig.8 that due to the NLO QCD corrections the differential cross section $d\sigma/d\cos\theta$ changes only with almost a common factor K as shown in TABLE III.

The energy-fraction distributions of B_c and B_c^* production, $\frac{d\sigma}{dz}$, are also computed with $\mu = 2m_b$, and the precise values obtained for the distributions are put into TABLE IV and in Fig.9 for the relevant curves. One may see from TABLE IV that the K factors vary with the energy-fraction z quite a lot, and from Fig.9 that the maximum point of the z distributions is shifted to smaller z due to QCD NLO corrections.

To see the asymmetry of the production caused by electroweak interaction i.e. to see the fact that the differential cross section, $d\sigma/d\cos\theta$, varies with the values of the electroweak mixing angle: $\sin^2\theta_w$, precisely, we take the B_c production as an example to compute the differential cross section, $d\sigma/d\cos\theta$, with various values of $\sin^2\theta_w$ ($\mu = 2m_b$) and the result is presented in Fig.10. As pointed out above, the NLO QCD corrections almost do not change the shape of the differential cross section for

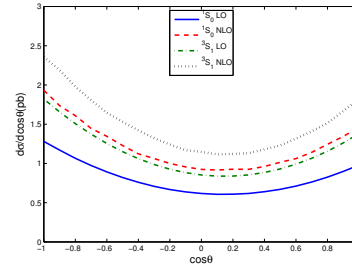


FIG. 8: The differential cross sections $\frac{d\sigma}{d\cos\theta}$ to LO and NLO for $e^-e^+ \rightarrow B_c(B_c^*) + b + \bar{c} + X$ at the Z pole ($\mu = 2m_b$).

the B_c production, except a K -factor, so here the differential cross section for NLO with $\mu = 2m_b$ in Fig.10 is approximately obtained by multiplying the relevant LO differential cross section with K -factor ($K \simeq 1.515$ for B_c production). From the figure one can see that the shape of the differential cross section is sensitive to the value of $\sin^2\theta_w$, thus the value of $\sin^2\theta_w$ may be measured precisely via observing the differential cross section of the production and/or the forward-backward asymmetry of the production.

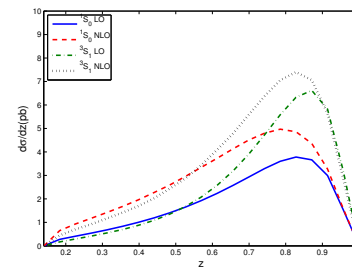


FIG. 9: The differential cross sections $\frac{d\sigma}{dz}$ to LO and NLO for $e^-e^+ \rightarrow B_c(B_c^*) + b + \bar{c} + X$ at the Z pole ($\mu = 2m_b$).

To see the variation of the total cross section with the collision energy \sqrt{s} around m_Z within 5 GeV, we also compute the cross section to LO and NLO with $\mu = 2m_b$ and put the result in TABLE V.

Here we should point out that the relevant decay widths respectively for the production of B_c and B_c^* by Z

decay, $\Gamma_{Z \rightarrow B_c(B_c^*)+b+\bar{c}+X}$, can be easily ‘read out’ from the total cross sections of the production, $\sigma(e^+e^- \rightarrow B_c(B_c^*)+b+\bar{c}+X)$, at Z pole, and in the literature there are the relevant decay widths, $\Gamma_{Z \rightarrow B_c(B_c^*)+b+\bar{c}+X}$, at LO and NLO[9, 10], thus we think that to have a very good check for the available results, precise comparisons of the widths induced from the total cross sections with those computed directly from the Z decay in literature should be carried out here. In Appendix-A, the way how to ‘read out’ the decay widths $\Gamma_{Z \rightarrow B_c(B_c^*)+b+\bar{c}+X}$ respectively from the total cross sections $\sigma(e^+ + e^- \rightarrow B_c(B_c^*)+b+\bar{c}+X)$ at Z pole is presented, and in Appendix-B careful comparisons up-to NLO are made. Unfortunately, the situation on the comparisons is that when we take the same input parameters exactly as those adopted in Refs.[9, 10], the induced NLO decay width $\Gamma_{Z \rightarrow B_c(B_c^*)+b+\bar{c}+X}$ is bigger than that in Ref.[9], but the in-

duced NLO decay width $\Gamma_{Z \rightarrow B_c(B_c^*)+b+\bar{c}+X}$ is consistent with that in Ref.[10].

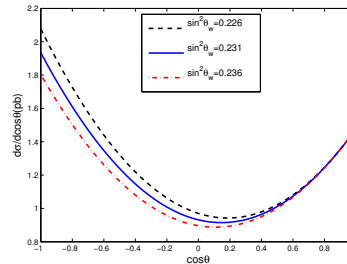


FIG. 10: The differential cross sections $\frac{d\sigma}{d \cos\theta}$ at the Z pole with various values of $\sin^2\theta_w$ ($\mu = 2m_b$).

$(\sqrt{s} - m_Z)(\text{GeV})$	-5	-2.5	-1.5	-0.8	-0.4	-0.2	0	0.2	0.4	0.8	1.5	2.5	5
B_c (LO)	0.09	0.30	0.63	1.10	1.42	1.53	1.58	1.54	1.44	1.13	0.66	0.32	0.10
B_c (NLO)	0.13	0.46	0.95	1.66	2.13	2.32	2.39	2.33	2.18	1.71	1.00	0.49	0.15
B_c^* (LO)	0.12	0.42	0.88	1.54	1.98	2.14	2.20	2.16	2.02	1.59	0.92	0.46	0.14
B_c^* (NLO)	0.16	0.56	1.17	2.04	2.64	2.84	2.93	2.87	2.67	2.11	1.23	0.60	0.18

TABLE V: The total cross sections (in pb) of $e^-e^+ \rightarrow B_c(B_c^*)+b+\bar{c}+X$ at various collision energies around m_Z ($\mu = 2m_b$).

$(\sqrt{s} - m_Z)(\text{GeV})$	-5	-2.5	-1.5	-0.8	-0.4	-0.2	0	0.2	0.4	0.8	1.5	2.5	5
B_c	0.18	-0.35	-0.63	-0.53	0.06	0.33	0.79	1.24	1.64	2.11	2.21	1.91	1.39
B_c^*	0.19	-0.53	-0.92	-0.78	-0.12	0.41	1.04	1.67	2.22	2.88	3.01	2.60	1.88

TABLE VI: The contributions (in fb) to the production due to the Feynman diagrams with a photon propagator to replace the Z -boson propagator at various collision energies around m_Z ($\mu = 2m_b$).

Since in the above calculations the contributions from the Feynman diagrams with a virtual γ , i.e. those Feynman diagrams in Fig.1 by replacing the Z -boson propagator with a photon one accordingly, are ignored. In order to see the contributions from the Feynman diagrams with a virtual γ , i.e. themselves squared and the interference of the Feynman diagrams with a Z -boson propagator and with a photon propagator, we compute the two parts precisely to QCD LO accuracy: the amplitude with a photon propagator squared and the interference of those with a Z -boson propagator and with a photon propagator, and put the results in TABLE VI. From the results TABLE VI one may see that the contributions from the ones with a photon propagator (those squared and the interference) around the resonance Z pole are very small in comparison with the contributions from those with a Z -boson propagator, thus it may be conclude that the approximation ignoring the contributions from the Feynman diagrams

with a virtual γ is quite good, furthermore since the precise values on the contributions estimated to QCD LO accuracy in TABLE VI are so small, so it is reasonable to believe that the conclusion will be still valid even the estimate on the contributions up-to QCD NLO accuracy.

V. DISCUSSIONS AND CONCLUSION

We have calculated the NLO QCD corrections to the production of B_c or B_c^* meson at e^+e^- colliders running near the Z pole. The results show that the NLO corrections are significant. The dependence on the renormalization scale μ for the cross sections at NLO level is suppressed in comparison with LO results. Precisely, the total cross section for the B_c (B_c^*) production at Z pole decreases about 46% (46%) for LO, and about 34% (30%) for NLO when μ changes from $2m_b$ to $m_Z/2$ ac-

cordingly. Namely, the dependence of the cross sections on the renormalization scale μ up-to NLO correction is still not small, so it means that the higher order QCD corrections may be requested.

In addition to the total cross sections, the differential cross sections on angle and energy fraction distributions of the produced $B_c(B_c^*)$ meson are computed and analyzed too. It is found that in the angle distribution the K -factor for NLO QCD accuracy to LO QCD accuracy changes slightly, but in energy distribution it changes sizable i.e. the maximum is shifted to smaller energy fraction (see TABLE. III, Figs. 8 and 9). The characters of the production up-to NLO accuracy in the differential cross sections in angle distribution are shown that they may be used to measure the electro-weak mixing angle $\sin^2\theta_w$.

According to the present NLO QCD calculations, the conclusion, that to study the production $e^+e^- \rightarrow B_c(B_c^*) + b + \bar{c} + X$ experimentally even at Z pole requests the collider to have its luminosity so high than $10^{35} \text{ cm}^{-2}\text{s}^{-1}$, still is valid, although it is established by LO calculations. It is because that the cross sections for the production even to QCD NLO accuracy are of the order $\mathcal{O}(pb)$, and the comparatively small efficiency in experimental detecting the meson $B_c(B_c^*)$.

Acknowledgments: We thank Jian-Xiong Wang and Rong Li for helpful discussions. This work was supported in part by Nature Science Foundation of China (NSFC) under Grant No. 11275243, No. 11275036, No. 11447601, No. 11535002 and No. 11675239

Appendix

A. The relation between the total cross sections $\sigma(e^+e^- \rightarrow B_c(B_c^*) + b + \bar{c} + X)$ at Z pole and decay widths $\Gamma(Z \rightarrow B_c(B_c^*) + b + \bar{c} + X)$

The total cross sections of the processes $e^+e^- \rightarrow Z \rightarrow B_c(B_c^*) + b + \bar{c} + X$ can be represented as

$$\sigma = \frac{1}{4} \frac{1}{2s} \frac{L^{\mu\nu} H_{\mu\nu}}{(s - m_Z^2)^2 + m_Z^2 \Gamma_Z^2}, \quad (21)$$

where Γ_Z is the total width of the boson Z , $L^{\mu\nu}$ is the leptonic tensor and

$$L^{\mu\nu} = a [q_1^\mu q_2^\nu + q_2^\mu q_1^\nu - (s/2)g^{\mu\nu}] + ibe^{\mu\nu\lambda\tau} q_{1\lambda} q_{2\tau}, \quad (22)$$

here

$$\begin{aligned} a &= \frac{e^2(1 - 4\sin^2\theta_w + 8\sin^4\theta_w)}{2\sin^2\theta_w \cos^2\theta_w}, \\ b &= \frac{e^2(1 - 4\sin^2\theta_w)}{2\sin^2\theta_w \cos^2\theta_w}. \end{aligned} \quad (23)$$

$H_{\mu\nu}$ is the hadronic tensor, which has been performed the phase space integration. $H_{\mu\nu}$ can only depend on k , and has following form

$$H_{\mu\nu} = H_1(s)g_{\mu\nu} + H_2(s)k_\mu k_\nu / s, \quad (24)$$

where $H_1(s)$ and $H_2(s)$ are scalar functions. Because there's no UV or IR divergence after considering the renormalization and the real correction, $H_1(s)$ and $H_2(s)$ are free of UV and IR divergences. Thus, all the derivations in the appendix are performed in 4 dimensions. According to Eqs.(21), (22) and (24), we can obtain the cross sections at Z pole

$$\sigma = -\frac{aH_1(m_Z^2)}{8m_Z^2 \Gamma_Z^2}, \quad (25)$$

here we have used $s = m_Z^2$.

The decay widths of the processes $Z \rightarrow B_c(B_c^*) + b + \bar{c} + X$ is

$$\Gamma = \frac{1}{3} \frac{1}{2m_Z} \Pi^{\mu\nu} H_{\mu\nu}, \quad (26)$$

where

$$\Pi^{\mu\nu} = -g^{\mu\nu} + k^\mu k^\nu / m_Z^2, \quad (27)$$

then we obtain

$$\Gamma = -\frac{H_1(m_Z^2)}{2m_Z}. \quad (28)$$

According to Eqs.(25) and (28), we obtain the relation

$$\Gamma = \frac{4m_Z \Gamma_Z^2}{a} \sigma. \quad (29)$$

Obviously from Eq.(29) one can obtain the decay widths for $Z \rightarrow B_c(B_c^*) + b + \bar{c} + X$ through the total cross sections of the processes $e^+e^- \rightarrow B_c(B_c^*) + b + \bar{c} + X$ which are calculated in the present paper.

B. To compare the results for the decay $Z \rightarrow B_c(B_c^*) + b + \bar{c} + X$ up-to NLO

There are NLO correction calculations on the decay widths for $Z \rightarrow B_c(B_c^*) + b + \bar{c} + X$ in Refs.[9, 10], so here we do the comparisons on the decay widths to NLO of theirs and those derived from our calculations on the total cross sections of the production $e^+e^- \rightarrow B_c(B_c^*) + b + \bar{c} + X$ in terms of the way in Appendix-A.

The two-cutoff phase space slicing method for the phase space integration by introducing δ_s [13] is used as indicated by Eqs.(9,10,11) and δ_s is fixed as 10^{-6} finally according to the requirement for the method. So it would be better that the errors generated by the calculations are presented precisely for the comparisons. Moreover, in order to compare the results in Refs.[9, 10] with ours, we take the same parameters as those taken in Refs.[9, 10] to compute the decay widths keeping the errors and put the results in TABLE VII and TABLE VIII.

μ	$\Gamma^{\text{LO+Vir+IR,soft}}$	$\Gamma_{\text{Real}}^{\text{IR,hard}}$	$\Gamma_{\text{Real}}^{\text{IR-finite}}$	Γ_{NLO}	$\Gamma_{\text{NLO}}(\text{Ref.}[9])$
$2m_b$	-567.60 ± 0.05	492.21 ± 0.07	186.44 ± 0.02	111.05 ± 0.09	78.45
$m_z/2$	-199.61 ± 0.02	200.05 ± 0.03	75.78 ± 0.01	76.22 ± 0.04	62.53

TABLE VII: The derived width (in keV) for the decay $Z \rightarrow B_c + b + \bar{c} + X$ from the total cross section for the relevant production $e^+ + e^- \rightarrow B_c + b + \bar{c} + X$ with the same input parameters as those in Ref.[9], and the values in the last column of the table are copied from Ref.[9]. Here for the derived NLO width, the statistical errors from numerical phase space integration are also presented.

μ	$\Gamma^{\text{LO+Vir+IR,soft}}$	$\Gamma_{\text{Real}}^{\text{IR,hard}}$	$\Gamma_{\text{Real}}^{\text{IR-finite}}$	Γ_{NLO}	$\Gamma_{\text{NLO}}(\text{Ref.}[10])$
$2m_b$	-632.78 ± 0.03	550.53 ± 0.07	200.73 ± 0.03	118.48 ± 0.09	118.77
$m_z/2$	-218.34 ± 0.02	221.90 ± 0.03	80.91 ± 0.02	84.47 ± 0.05	84.60

TABLE VIII: The derived width (in keV) for the decay $Z \rightarrow B_c^* + b + \bar{c} + X$ from the total cross section for the relevant production $e^+ + e^- \rightarrow B_c^* + b + \bar{c} + X$ with the same input parameters as those in Ref.[10], and the values in the last column of the table are copied from Ref.[10]. Here for the derived NLO width, the statistical errors from numerical phase space integration are also presented.

From the tables, one may see that the results for NLO corrections of B_c production in [9] are different from ours,

but those for NLO corrections of B_c^* production in [10] are consistent with ours.

-
- [1] F. Abe, et al. (CDF Collaboration), Observation of the B_c Meson in $p\bar{p}$ Collisions at $\sqrt{s} = 1.8\text{TeV}$, Phys. Rev. Lett. **81**, 2432 (1998); Observation of B_c mesons in $p\bar{p}$ collisions at $\sqrt{s} = 1.8\text{TeV}$, Phys. Rev. D **58**, 112004 (1998).
- [2] E.J. Eichten and C. Quigg, Mesons with beauty and charm: Spectroscopy, Phys.Rev. D**49**, 5845 (1994).
- [3] G.T. Bodwin, E. Braaten and G.P. Lepage, Rigorous QCD analysis of inclusive annihilation and production of heavy quarkonium, Phys. Rev. D **51**, 1125 (1995) [Erratum-ibid. D **55**, 5853 (1997)].
- [4] N. Brambilla, et al. Heavy Quarkonium Physics, CERN-2005-005 20 June 2005, arXiv: hep-ph/0412158.
- [5] N. Brambilla, et al. Heavy quarkonium: progress, puzzles, and opportunities, Eur. Phys. J. C **71**, 1534 (2011) and references therein.
- [6] C.-H Chang and Y.-Q Chen, The Production of B_c or \bar{B}_c associated with two heavy quark jets in Z^0 boson decay, Phys. Rev. D **46**, 3845 (1992); Erratum, Phys. Rev. D **50**, 6013 (1994); The B_c and \bar{B}_c mesons accessible to experiments by Z^0 boson decay, Phys. Letts. B **284**, 127-132 (1992).
- [7] P. Abreu, et al (DELPHI Collaboration), Search for the B_c meson, Phys. Letts. B **398**, 207 (1997); R. Barate, et al (ALEPH Collaboration), Search for the B_c meson in hadronic Z^0 decay, Phys. Letts. B **402**, 213 (1997); K. Ackerstaff, et al (OPAL Collaboration), Search for the B_c meson in hadronic Z^0 decay, Phys. Letts. B **420**, 157 (1998).
- [8] X.-C. Zheng, C.-H. Chang and Z. Pan, Production of doubly heavy-flavored hadrons at e^+e colliders, Phys. Rev. D **93**, 034019 (2016).
- [9] C.-F. Qiao, L.-P. Sun, R.-L. Zhu, The NLO QCD Corrections to B_c Meson Production in Z^0 Decays, JHEP **08**, 131 (2011).
- [10] J. Jiang, L.-B. Chen, C.-F. Qiao, QCD NLO corrections to inclusive B_c^* production in Z^0 decays, Phys. Rev. D**91**, 034033 (2015).
- [11] M. Beneke and V.A. Smirnov, Asymptotic expansion of Feynman integrals near threshold, Nucl. Phys. B**522**, 321 (1998).
- [12] J.G. Korner, D. Kreimer and K. Schilcher, A Practicable γ_5 -scheme in dimensional regularization, Z. Phys. C**54**, 503 (1992).
- [13] T. Kinoshita, Mass Singularities of Feynman Amplitudes, J. Math. Phys. **3**, 650 (1962).
- [14] S. Dittmaier, Separation of soft and collinear singularities from one-loop N-point integrals, Nucl. Phys. B**675**, 447 (2003).
- [15] G. Grammer, Jr. and D. R. Yennie, Improved Treatment for the Infrared-Divergence Problem in Quantum Electrodynamics, Phys. Rev. D **8**, 4332 (1973).
- [16] B.W. Harris and J.F. Owens, Two cutoff phase space slicing method, Phys. Rev. D **65**, 094032 (2002).
- [17] A. Bassetto, M. Ciafaloni, and G. Marchesini, Jet Structure and Infrared Sensitive Quantities in Perturbative QCD, Phys. Rept. **100**, 201 (1983).
- [18] A. Denner, Techniques for the Calculation of Electroweak Radiative Corrections at the One-loop Level and Results for W-physics at LEP-200, Fortschr. Phys. **41**, 307 (1993).
- [19] K.A. Olive, et al. (Particle Data Group), Review of particle physics, Chin.Phys. C**38**, 090001 (2014).
- [20] T. Hahn, Generating Feynman diagrams and amplitudes with FeynArts 3, Comput. Phys. Commun **140**, 418 (2001).

- [21] R. Mertig, M. Bohm and A. Denner, Feyn Calc - Computer-algebraic calculation of Feynman amplitudes, *Comput. Phys. Commun* **64**, 345 (1991).
- [22] F. Feng and R. Mertig, FormLink/FeynCalcFormLink: Embedding FORM in Mathematica and FeynCalc, arXiv:1212.3522.
- [23] F. Feng, \$Apart: A Generalized Mathematica Apart Function, *Comput. Phys. Commun* **183**, 2158 (2012).
- [24] A.V. Smirnov, Algorithm FIRE - Feynman Integral Reduction, *J. High Energy Phys.* **10**, 107 (2008).
- [25] T. Hahn and M. Perez-Victoria, Automatized one loop calculations in four-dimensions and D-dimensions, *Comput. Phys. Commun* **118**, 153 (1999).
- [26] G.P. Lepage, A New Algorithm for Adaptive Multidimensional Integration, *J. Comp. Phys.* **27**, 192 (1978).